Internal Stresses during Film Formation of Polymer Latices

Christian Petersen,[†,‡] Carsten Heldmann,[§] and Diethelm Johannsmann*[,‡]

Max-Planck-Institute for Polymer Research, Ackermannweg 10, D-55128 Mainz, Germany, and Clariant GmbH, D-65926 Frankfurt, Germany

Received March 4, 1999. In Final Form: June 11, 1999

The lateral stresses that latex dispersions undergo upon forming films have been investigated by an optical lever technique. Dilational lateral stress induced by capillary pressure, tensile stress caused by the uniaxial shrinkage imposed by the substrate, and stress relaxation on longer time scales were observed. Failure of film formation because of cracking events was reflected in irregular substrate deflection. The stress evolution in pigment-filled paints below the critical pigment volume concentration displayed two maxima in tensile stress which we associate with a separation of time scales between the drying of polymeric binder and the particle rearrangement to eliminate voids.

Introduction

During film formation polymer latices undergo an irreversible change from a stable colloidal dispersion to a continuous, transparent, and mechanically stable film.[1,2] The process of film formation is usually divided into three stages. Stage I is evaporation, in which the dispersion increases in density until the particles touch. The particles then undergo deformation to polyhedra in stage II. In stage III, the boundaries between the particles disappear through the interdiffusion of polymer chains, and the film develops its final toughness and strength.[3]

The micromechanical processes during particle deformation have been the subject of considerable debate.[4−8] Dillon et al. were the first to address this issue in 1951.[9] These authors suggested that particle deformation was driven by polymer−air interfacial tension (dry sintering). Vanderhoff et al. postulated an analogous mechanism based on the polymer−water interfacial tension (wet sintering).[10,11] Capillary pressure as the driving force of coalescence was suggested by Brown.[12] An important common consequence of these considerations is that film formation is only possible with sufficiently soft latices. This correlates with the experimental finding of a "minimum film-forming temperature" (MFT),[13] below which the material stays brittle and turbid instead of transforming into a homogeneous film. The MFT is usually close to (but not necessarily identical with) the glass temperature T_g of the polymer.[14] Below this temperature the spheres are too rigid to undergo deformation and coalescence. Both particle deformation and interdiffusion may be assisted by low molecular weight plasticizers or "coalescing aids."[15]

The evolution of stress during film formation has rarely been probed experimentally. In view of the considerable importance of mechanical stress for film formation and durability,[16] this seems somewhat surprising. On a qualitative basis, the stress in drying paints is sometimes monitored via the bending of flexible foils used as substrates.[17] Obviously, the experimentally accessible stresses are macroscopic in nature and result from an integration over the entire sample. However, the connection of this bulk effect to the micromechanical phenomena can be made. We have used a cantilever method to follow the macroscopic stress evolution. The films are dried on a flexible substrate, which bends under the influence of stress. The substrate curvature is detected with a laser beam reflected from a small mirror attached to its end. This classical technique has been used previously to measure the stresses caused by thermal expansion and uptake of water.[18,19] It also has been applied in solid-state physics, where surface stress differences (for instance, caused by surface reconstruction) have been studied.[20−22] Recently, the interest in bending plate techniques has been renewed by the availability of microfabricated cantilevers.[23−25] The technique has the

† Present address: Grinnell College, 10-32 Grinnell, Iowa 50112, USA.

‡ Max-Planck-Institute for Polymer Research.

§ Clariant GmbH.

* To whom correspondence should be sent. Phone: 49-6131-379 163. E-mail: johannsmann@mpip-mainz.mpg.de. Fax: 49-6131-379 360.

(1) Keddie, J. L. *Mater. Sci. Eng. Rep.* **1997**, *21*, 101.
(2) Winnik, M. A. *Curr. Opin. Colloid Interface Sci.* **1997**, *2*, 192.
(3) Vanderhoff, J. W.; Bradford, E. B.; Carrington, W. K. *J. Polym. Sci.* **1973**, *41*, 155.
(4) Richard, J. *Polymer* **1992**, *33*, 562.
(5) Richard, J.; Maquet, J. *Polymer* **1992**, *33*, 4164.
(6) Richard, J. *Polymer* **1993**, *34*, 3823.
(7) Dobler, F.; Holl, Y. *Trend. Polym. Sci.* **1996**, *4*, 145.
(8) Lin, F.; Meier, D. J. *Langmuir* **1996**, *12*, 2774.
(9) Dillon, R. E.; Matheson, L. A.; Bradford, E. B. *J. Colloid Sci.* **1951**, *6*, 108.
(10) Vanderhoff, J. W.; Tarkowski, H. L., Bradford, E. B. Presented to Division of Organic Coatings and Plastics Chemicals, at 149th Meeting of the American Chemical Society, 1965, Preprints **1965**, *25*, 319.
(11) Vanderhoff, J. W. *Br. Polym. J.* **1970**, *2*, 161.
(12) Brown, G. L. *J. Polym. Sci.* **1956**, *22*, 423.
(13) Potzman, T. F.; Brown, G. L. *J. Appl. Polym. Sci.* **1960**, *4*, 81.
(14) Brodnyan, J. G.; Konen, T. *J. Appl. Polym. Sci.* **1964**, *8*, 687.
(15) Juhué, D.; Wang, Y.; Winnik, M. A.; Haley, F. *Makromol. Chem. Rapid. Commun.* **1993**, *14*, 861.
(16) Perera, D. Y. *Prog. Org. Coat.* **1996**, *28*, 21.
(17) Dörr, H.; Holzinger, F. *Kronos Titanium Dioxide in Emulsion Paints, Optimal Formulation for Quality and Efficiency*; Kronos International, Peschstr. 5, Leverkusen, Germany, Druckereigesellschaft mbH, Dortmund, p 63 ff.
(18) Zosel, A. *Lack- und Polymerfilme: Viskoelastische Qualitätsmerkmale*; Curt Vincent Verlag: Hannover 1996; p 113.
(19) Perera, D. Y.; Vanden Eynde, D. *J. Coat. Technol.* **1987**, *59*, 55.
(20) For a review see Butt, H.-J.; Raiteri, R. In *Surface Characterization: Principles, Techniques and Applications*; Milling, Ed.
(21) Cahn, J. W.; Hannemann, R. E. *Surf. Sci.* **1964**, *1*, 387.
(22) Finn, M. C.; Gatos, H. C. *Surf. Sci.* **1964**, *1*, 361.
(23) Butt, H.-J. *J. Colloid Interface Sci.* **1996**, *180*, 251.
(24) Chen, G. Y.; Thundat, T.; Wachter, E. A.; Warmack, R. J. *J. Appl. Phys.* **1995**, *77*, 3618.
(25) Lang, H. P.; Berger, R.; Battiston, F.; Ramseyer, J. P.; Meyer, E.; Andreoli, C.; Brugger, J.; Vettiger, P.; Despont, M.; Mezzacasa, T.; Scandella, L.; Güntherodt, H. J.; Gerber, C.; Gimzewski, J. K. *Appl. Phys. A* (*Mater. Sci. Proc.*) **1998**, *66* (Part 1 Suppl. S), 61.

10.1021/la990256m CCC: $18.00

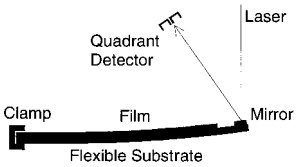

Figure 1. Schematic description of the experimental setup.

potential of extreme sensitivity, although the experiments reported here are actually undemanding in this respect. Compared with the drying of conventional polymers, the stress evolution encountered during drying of latex films is much more complex, which is indicative of a multitude of micromechanical processes.

Materials

Most of the experiments were carried out on a model latex based on poly(vinyl acetate) (PVAc). This material was synthesized specifically for research purposes and therefore designed with the greatest possible simplicity as far as additives and components are concerned. Details of the preparation are described in refs 26 and 27. The particle size was $d_w = 130$ nm as determined with photocorrelation spectroscopy, and the size dispersity was $d_w/d_n = 1.08$. Stabilization against aggregation was achieved by the copolymerization of 0.5% sodium vinyl sulfonate. In addition, sodium tri(*tert*-butyl)phenol oligoethylene glycol sulfate (Hostapal BV) was added as emulsifier in a concentration of 3 wt % with regard to the monomer VAc. The solid content was 51.5%. The glass transition temperature as determined with differential scanning calorimetry was 40 °C. The MFT was measured with a temperature gradient bar at 19 °C. The experiments were carried out at temperatures higher than the MFT.

For the investigation of film formation failure, we used a core−shell system with a sample code KR59. The soft core (60 wt %) is a copolymer of 70% butyl methacrylate (BuMA) and 30% butyl acrylate (BuA). The hard shell (40 wt %) is a copolymer of 90% methyl methacrylate (MMA) and 10% BuMA. The stabilizing agent was sodium dodecyl sulfate (SDS) in a concentration of 1.5%. The solid content was 50% and the particle size was 94 nm. The film formation properties of this compound are rather complex and will be reported in detail in a separate publication.[28] Important in the context of this work is the fact that cracks evolve unless the dispersion is dried very slowly or at temperatures much higher than 44 °C. Strictly speaking, 44 °C is not an MFT because stable films do form at even lower temperatures provided that the system is given enough time.

To investigate the influence of pigment loading, experiments on paints with varying pigment concentration were also performed. The mill base was a mixture of 6.25 parts of TiO_2 and 3.75 parts of $CaCO_3$, where hydroxyl ethyl cellulose ether was used as thickener. The binder in this case was a vinyl acetate/ethylene dispersion. The use of ethylene as comonomer ensured an MFT below room temperature. The volume concentrations spanned from 27 to 81%, covering the region from well below the critical pigment volume concentration (CPVC), where the pigment is dispersed in a matrix of polymeric binder, to well above the CPVC, where the binder is just sufficient to interconnect the pigment particles, the rest of the volume being filled with air. The CPVC of this system was determined from gloss and foil-bending measurements to be (55 ± 3) %.[17]

Experimental Section

The experimental setup is sketched in Figure 1. A Helium−Neon laser beam is deflected from the end of a 28-mm-long and 100-μm-thick metal strip on which the latex dispersion is applied with a pulling bar. This substrate bends under the influence of the drying-induced stress, which leads to a slight movement of the reflected laser beam. The beam is reflected from a 5 mm × 10 mm silica mirror glued to the end of the substrate, and the position of the reflected beam is monitored with a quadrant detector (JQ 5OP from Laser Components). From the beam deflection the stress in the film is derived.

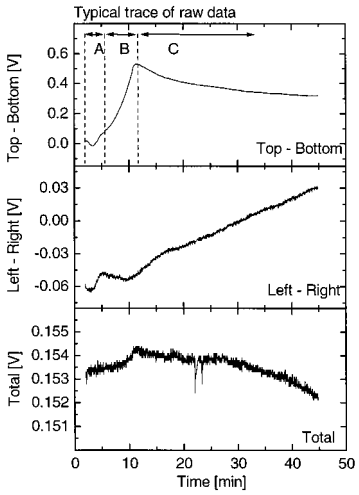

Figure 2. Typical trace of raw data taken on a 15-μm PVAc film. "Total" is the sum of all detector outputs. "Top − Bottom" is the normalized difference between the two upper and the two lower detectors in volts. "Left − Right" is the normalized difference between the two left and the two right detectors. As expected from an essentially vertical movement of the substrate, the variation in "Top − Bottom" is larger than the "Left − Right" signal. We distinguish between an initial phase with dilational stress (A), a second phase with a maximum in tensile stress (B), and stress relaxation on longer time scales (C).

The length of the substrate was chosen to achieve maximum sensitivity, which scales linearly with the substrate length, while minimizing any undesirable influence of the film weight on substrate bending. The latter effect scales with the cube of the substrate length and can largely be eliminated with sufficiently short substrates.

The metal used was a strip of bronze purchased from Goodfellow. Bronze was the only substrate available to us which had been shipped in straight sheets rather than in rolls. It was preferable to use straight sheets because there appeared to be some internal stress relaxation dynamics with curved substrates. Apart from the issue of curvature, different materials (steel, brass, copper) behaved in essentially the same manner.

Figure 2 shows a trace of the raw data. "Total" is the sum of all detector outputs. The variation of about 1% in the "Total" signal could come from many different sources such as fluctuations in laser intensity, different responsivity of the four detectors, blind boundary regions between the detectors, etc. We do not attribute any significance to these variations. "Top − Bottom" is the normalized difference between the two upper and the two lower detectors. "Left − Right" is the normalized difference between the two left and the two right detectors. As expected for an essentially vertical movement, the variation in the "Top − Bottom" signal is larger than in the "Left − Right" signal, the latter corresponding to a twisting movement. A small amount of substrate twisting is expected because the drying proceeds somewhat unevenly across the surface. Calibration of the quadrant detector was carried out by changing its vertical position by known amounts with an optical stage. Applying straightforward algebra, the "Top − Bottom" signal is converted to a deflection angle γ. The deflection angle γ is the central observable of the experiment. The noise level and the range of linearity are 0.001° and 0.2°, respectively.

To convert the substrate deflection to a stress difference, the stiffness of the substrate has to be known. It is determined by placing a known weight onto the end of the substrate and measuring the induced deflection γ_L. Beam theory states that

(26) Du Chesne, A.; Bojkova, A.; Stöckelmann, E.; Krieger, S.; Heldmann, C. *Acta Polym.* **1998**, *49*, 346.

(27) *Filmbildung wässriger Kunststoffdispersionen.* Abschlussbericht BMBF−Vorhaben FKZ 03N3018 A 5, Deutsche Forschungsberichte, University Bibl. U. TIB Hannover 1997.

(28) Du Chesne, A.; Bojkova, A.; Rottstegge, J.; Glasser, G.; Neher, D.; Krieger, S., Manuscript in preparation.

the deflection γ_L depends on the product of the substrate's Young's modulus E_s and the cube of the substrate thickness t_s^3.[29] We could not accurately measure the substrate thickness directly with a caliper because of the presence of dust grains. Instead, we used the Young's modulus given by the supplier ($E_s = 90-110$ GPa) and calculated the substrate thickness from the beam deflection under the load γ_L and the Young's modulus. The resulting value of $t_s \approx 100$ μm is consistent with the thickness as estimated with a caliper.

The initial thickness of a drying film is given by the gap width of the pulling bar. The final ("dry") thickness is calculated from the initial film thickness and the known solid content of the dispersion. In some qualitative investigations we also used steel substrates which are reflective themselves. In these experiments the beam passed through the drying film and was reflected from both the film−air interface and the substrate−film interface, causing optical interference fringes. Although these experiments yield inferior data quality, they offer the attractive feature that the film thickness can be calculated from the interference fringes at any time during drying.

The setup is contained in a plastic hood to ensure relatively constant temperature and humidity as well as to limit the effect of air currents. Temperature and humidity are monitored with the P570 sensor from Dorstmann Electronics. Typical values for the humidity were between 35 and 50 %rH. After each experiment the hood was taken off to maintain approximately the same relative humidity. As expected, the speed of drying depended on humidity. During an experiment the film is pulled out by hand with a pulling bar (Erichsen) onto the bronze substrate which rests on top of a variable temperature plate. The substrate is then partly pushed over the edge of the plate, and a weight is placed on top of it. The configuration is then analogous to a beam clamped on one side treated in many textbooks on elasticity.[29] The position of the quadrant detector is adjusted to place the beam properly on it, and data acquisition starts 1 min after pulling the film. Because of the time necessary to ready the setup after pulling the film, the stress history during the first minute is unknown. Data are read out about once a second.

Control experiments were performed on the substrate alone to test for temperature dependence, susceptibility to air currents, and long-term drift. A control experiment was performed in which the substrate was hit quickly, and the relaxation time was monitored to ensure that the internal stress relaxation dynamics of the substrates were insignificant. The substrate was examined under light microscopy over several experiments to confirm that there was no accumulation of residual films.

Data Analysis

Calculation of Equivalent Stress. Before proceeding to the mathematics of the stress derivation, some caveats with regard to the formalism must be mentioned. First, the experiment as it is carried out here only determines the *integral* stress (or rather the "force per unit width"), not the local stress. In fact, the observed thickness dependence of the maximum force indicates an inhomogeneous distribution of internal stress as suggested by the Sheetz model.[30] Second, it should be pointed out that the experiment is sensitive to *lateral* stress, as opposed to vertical stress or hydrostatic pressure. Finally, the zero-stress position of the cantilever unfortunately cannot be determined. The quadrant detector is optimized for maximum signal during the first minute of each experiment, and there is no way of reaching a stress-free situation once the experiment has started. We arbitrarily set the origin of the stress scale to the beginning of data acquisition.

Because of the bending of the substrate, the stress measurements do not occur under constant deformation. In principle, bending relaxes part of the stress. However, this is a very small effect. The maximum elongation ϵ_{max} is given by $\gamma_{max}\, t_s/(2L) \approx 6 \times 10^{-6}$. Multiplying this deformation by any reasonable Young's modulus of the film (say $E_f < 100$ MPa), one finds that the associated stress relaxation amounts to at most 500 Pa. This is negligible compared with the other stresses encountered in this experiment which are on the order of megapascals.

We assume a no-slip condition at the substrate−film interface. The dispersions investigated here are sticky materials. They are designed to be used as binders in the formulation of paints and other loaded materials. Actually, interfacial slippage between suitably chosen substrate−film pairs might be an interesting topic to be addressed with the same technique. However, it is not part of the picture in this work.

With the above-mentioned caveats admitted, we still consider it useful to convert the observed bending of the cantilever to an "equivalent stress." Again, the equivalent stress is to be understood as an averaged quantity. The relation between substrate deflection and equivalent stress follows from standard force balance considerations.[29] The sample consists of a composite beam of length L and width w with a substrate of thickness t_s and film of thickness t_f. The equivalent stress in the film σ_f is assumed to be constant, independent of the vertical position z. Under the influence of stress the substrate bends with radius of curvature R. The curvature is constant along the substrate and given by $1/R = \gamma/L$. Bending elongates the sheets in the upper section of the substrate and compresses the sheets in the lower section. Between the elongated and the compressed parts there is a "neutral fiber" at the position z_n. The local elongation is $\epsilon_s = (dx - dx_0)/dx_0$ with dx and dx_0 the infinitesimal length along the long axis of the substrate in the deformed and the undeformed state, respectively. The deformation $\epsilon_s(z)$ is given by

$$\epsilon_s(z) = \frac{(z - z_n)}{R} \tag{1}$$

In the substrate, deformation results in a local stress $\sigma_s(z)$ given by

$$\sigma_s(z) = E_s \epsilon_s(z) = E_s \frac{(z - z_n)}{R} \tag{2}$$

where E_s is the Young's modulus of the substrate.[31]

The position of the neutral sheet z_n is derived from the condition that there is no net elongational force acting on the substrate:

$$0 = \frac{1}{R}\int_0^{t_s} E_s(z - z_n)\, dz + \int_{t_s}^{t_s+t_f} \sigma_f\, dz \tag{3}$$

which results in

$$z_n = \frac{t_s}{2} + \frac{R\sigma_f\, t_f}{E_s t_s} \tag{4}$$

The radius of curvature R is derived from the condition that there is no external torque acting on the substrate:

$$0 = \frac{1}{R}\int_0^{t_s} E_s(z - z_n)^2\, dz + \int_{t_s}^{t_s+t_f} \sigma_f(z - z_n)\, dz \tag{5}$$

which results in

(29) Landau, L. D.; Lifshitz, E. M. *Lehrbuch der theoretischen Physik*; Akademie Verlag: Berlin, 1983; Vol 7, p 48.

(30) Sheetz, D. P. *J. Appl. Polym. Sci.* **1965**, *9*, 3759.

(31) A somewhat subtle issue is the question which modulus should be used. If the substrate is considered to be constrained in the plane pependicular to the direction of bending, $E_s/(1 - \nu)$ with ν the Poisson's number should be used instead of the Young's modulus E_s.

$$\sigma_f = \frac{E_s t_s^3}{6 t_f R (t_s + t_f)} = \frac{E_s t_s^3}{6 t_f (t_s + t_f) L}\,\gamma \tag{6}$$

To emphasize the fact that only changes in the deflection angle γ are measured, one can also write

$$\Delta\sigma_f = \frac{E_s t_s^3}{6 t_f (t_s + t_f) L}\,\Delta\gamma \tag{7}$$

Ideally, the thickness of the film should be measured parallel with the stress. This is indeed possible by observing the interference fringes from a film on a reflecting substrate.

An interesting limit occurs, when the film thickness is much less than the thickness of the substrate, that is $t_f \ll t_s$. In this case eq 4 is approximated by

$$z_n \approx \frac{t_s}{2} \tag{8}$$

eq 5 simplifies to

$$0 \approx \frac{1}{R}\int_0^{t_s} E_s\left(z - \frac{t_s}{2}\right)^2 \mathrm{d}z + \frac{t_s}{2}\int_{t_s}^{t_s+t_f} \sigma_f \,\mathrm{d}z \tag{9}$$

and eq 7 reads

$$\Delta\left(\int_{t_s}^{t_s+t_f} \sigma_f \,\mathrm{d}z\right) \approx \frac{E_s t_s^2}{6L}\,\Delta\gamma \tag{10}$$

Equation 10 is the equivalent of Stoney's formula.[32] Under the condition $t_f \ll t_s$, the curvature is directly proportional to the integral stress or "force per unit width." The integral has the dimensions of a surface energy and in fact may be viewed as such. The condition $t_f \ll t_s$ was fulfilled for most of the experiments.

The average stress can be derived as

$$\Delta\sigma_f \approx \frac{E_s t_s^2}{6 t_f^{av} L}\,\Delta\gamma \tag{11}$$

The arithmetic mean of the initial and the final film thickness was used for t_f^{av}. The solid content of the dispersions is on the order of 0.5. Therefore, using the average film thickness instead of the instantaneous thickness introduces an error of at most 50%. Equation 11 was used for the calculation of the equivalent stresses displayed in Figures 5−8. For a 15-μm film, a declination of 0.1° corresponds to an average stress of 1 MPa.

The Young's modulus of the substrate E_s was used as given by the manufacturer. The thickness of the substrate t_s was calibrated by placing a weight of known mass m_L onto the end of the substrate. The torque balance equation for this case results in

$$\gamma_L = \frac{6 g m_L L^2}{w}\,\frac{1}{E_s t_s^3} \tag{12}$$

where γ_L is the deflection angle induced by the weight m_L, $g = 9.81$ m s^{-2} is the earth's gravitational constant, and $w = 59$ mm is the width of the substrate. The substrate thickness t_s derived from eq 12 is inserted into eq 11 when calculating the lateral stress.

Effect of the Mass Loss. In principle, the measured change in deflection may result from both the internal stress and the evaporative loss of the film's water mass. The film's weight exerts an external torque and the left-hand side of eq 5 is no longer zero. In the following, we estimate the influence of mass loss. For clarity we omit the stress in this calculation. The two effects are additive. With a film of finite weight placed on the substrate surface the torque balance equation at any point x is given by

$$\frac{1}{R_w(x)}\int_0^{t_s} E_s (z - z_n)^2 \,\mathrm{d}z = \int_x^L g\rho t_f (\xi - x)\,\mathrm{d}\xi \tag{13}$$

with $1/R_w(x)$ the curvature induced by the weight, x the spatial coordinate along the long axis of the substrate, and ρ the mass density of the film. Assuming $z_n \sim t_s/2$, eq 13 is solved by

$$R_w(x) = \frac{E_s t_s^3}{6}\,\frac{1}{g\rho t_f (L - x)^2} \tag{14}$$

Note that the curvature is not constant along the substrate in this case. The substrate deflection at the end of the substrate γ_w is

$$\gamma_w = \int_0^L \frac{1}{R_w(x)}\,\mathrm{d}x = \frac{2 g\rho t_f L^3}{E_s t_s^3} \tag{15}$$

The relative contribution of the weight γ_w/γ (cf. eq 6) is then given as

$$\frac{\gamma_w}{\gamma} = L^2\,\frac{g\rho}{3\sigma_f (t_s + t_f)} \tag{16}$$

The relative contribution of film weight scales as the square of the substrate length, which motivates the use of short substrates. Inserting typical values ($\rho = 10^3$ kg m^{-3}, $t_f = 30$ μm), one arrives at $\gamma_w \sim 0.007$ °. Also, note that most of the mass loss occurs in the very early phase of the experiment. Stress dominates the picture.

Results and Discussion

A typical trace of the raw data is shown in Figure 2. This particular experiment was conducted on a 15-μm PVAc film. Here and in the following all thicknesses are to be understood as initial thicknesses as given by the gap width of the pulling bar. The different features observed are summarized as follows:

Phase A. This period of declination corresponds to dilational lateral stress, the magnitude of which varies considerably between the different experiments. This phenomenon is not observed in the drying of conventional polymers.

Phase B. This is a maximum of tensile stress.

Phase C. This phase is a long-term relaxation of tensile stress, the end of which frequently was beyond the time scale of the experiment.

To connect the different phases with internal processes of film formation we seek to correlate the stress history with the instantaneous film thickness. Figure 3 shows a data trace from an experiment in which the use of a reflective substrate allowed for this observation. From the frequency of the fringes in the "Total" signal one sees that the thickness decreases linearly until about the

(32) Stoney, G. G. *Proc. R. Soc. London. Ser. A* **1909**, *82*, 172. Stoney considers a symmetric configuration with slightly different boundary conditions. An additional factor of $(1 - \nu)$ with ν the Poisson's number enters in the denominator.

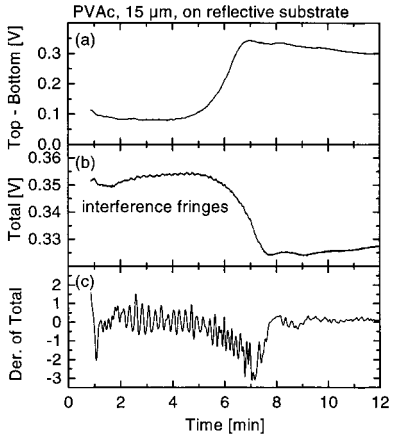

Figure 3. Data taken on reflective steel substrates displaying interference fringes in the "Total" channel. (a) substrate declination; (b) substrate reflectivity; (c) derivative of b to visualize the interference fringes. The fringes result from interference between the beams reflected at the film−air and the substrate−film interface. The speed of drying can be estimated from the frequency of the interference fringes. The drying process slows down considerably at the maximum of tensile stress.

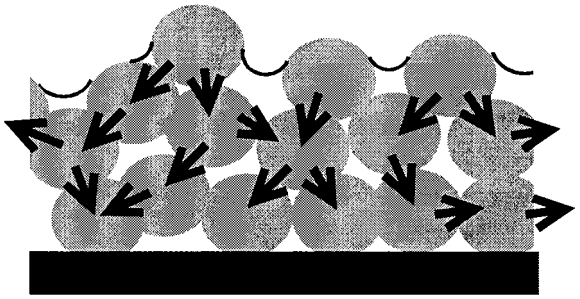

Figure 4. Schematic drawing of the mechanism by which capillary stress propagates through an ensemble of spheres touching each other. There is a net dilational lateral stress bending the substrate *downward*.

maximum of tensile stress (end of phase B) where the interference fringes slow down and eventually disappear. The overall number of fringes matches what one expects from the initial and the final film thickness as calculated from the solid content of the dispersion. The linear decrease in film thickness is assigned to stages I and II (evaporation and particle deformation) in the standard picture of film formation. Therefore we identify the time of maximum tensile stress with the end of stage II. Phase C corresponds to stage III, which is interdiffusion. Because the solid content of the dispersion is close to the limit of stability, stage I (evaporation) passes very quickly. Presumably, the particles have touched already, when the measurement starts ($t \sim 1$ min).

We assign the declination of the substrate observed in phase A to capillary pressure. Inside structured media a liquid−air interface can exert a substantial force. It has been shown that capillary forces qualitatively change the drying behavior of droplets containing colloidal particles.[33] Figure 4 illustrates how capillary pressure can result in a net dilational lateral stress which bends the substrate downward. To further support our hypothesis, we show the stress evolution in a drying film of a poly(methyl methacrylate) (PMMA) polymer film from solution in toluene in Figure 5. No dilational stress is observed. This is expected because conventional polymers do not contain

(33) Deegan, R. D.; Bakajin, O.; Dupont, T. F.; Huber, G.; Nagel, S. R.; Witten, T. A. *Nature* **1997**, *389*, 827.

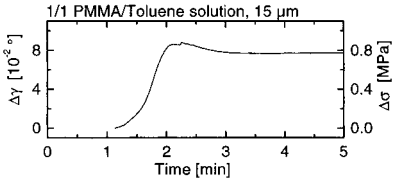

Figure 5. Drying history of polymer film of poly(methyl methacrylate) (PMMA). The material is a conventional polymer, not a latex dispersion. No dilational stress is observed. Dilational lateral stress evidently is connected to particle deformation, which naturally does not occur for conventional polymers. The other phases (tensile stress caused by uniaxial shrinkage and stress relaxation) occur in the same way as for lattices.

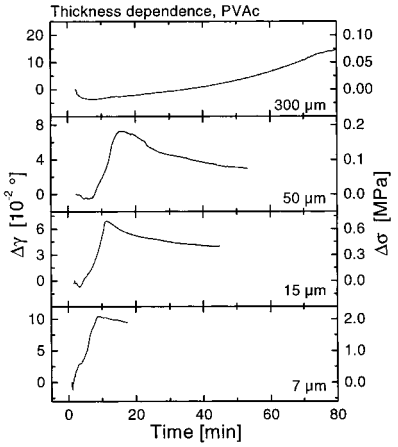

Figure 6. Evolution of average stress calculated according to eq 11 for a series of PVAc films with different thicknesses. As expected, drying is slower for thicker films. The qualitative appearance is similar for the different thicknesses. The origin of the scale of equivalent stress has been set arbitrarily to the stress at the beginning of data acquisition.

internal cavities and do not allow for the formation of a curved meniscus.

It is instructive to calculate the maximum lateral stress that capillary pressure can possibly exert. Capillary pressure amounts to at most 1 atm (= 10^5 Pa). Treating the assembly of interconnected spheres as a single elastic medium, one can write $\sigma_{lat} = \nu\, \sigma_{norm}$ with σ_{lat} the lateral pressure, σ_{norm} the normal pressure, and ν the effective Poisson's number of the medium. ν should be substantially larger than zero (finite elasticity) and less than 1/2 (ideal rubber elasticity). A vanishing Poisson's number would correspond to a perfectly rigid skeleton of spheres, which is certainly unrealistic. The condition of $\nu < 1/2$ follows from the requirement that both the shear modulus and the bulk modulus of compression are positive. Any kind of effective medium will fulfill this assumption. According to this calculation the maximum lateral stress exerted by capillary pressure should be of the order of 0.05 MPa. As Figure 6 shows, experiment is in accordance with this estimate. The larger declinations visible in Figure 8, on the other hand, are too strong to be compatible with an interpretation in terms of capillary pressure.

The interpretation given above should not apply for very thin films if the arguments advanced by Sheetz in 1965 are correct.[30] Sheetz pointed out that because of the finite contact angle, the meniscus will not only exert vertical pressure but also pull together the particles at the film−air interface. He concluded that the lateral tension will result in the formation of a continuous skin at the film−air interface. The skin acts like a piston exerting vertical pressure onto the underlying material. In this picture, the air−water interface exerts *tensile stress in the topmost*

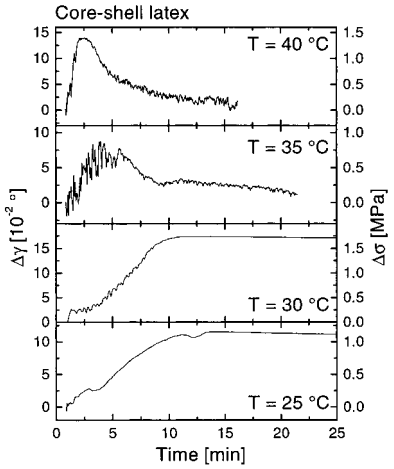

Figure 7. Stress histories as a function of temperature for the drying of a core−shell latex with an initial thickness of 15 μm. This material cracks extensively when dried at a temperature below 44 °C.[28] The fluctuations occurring on the time scale of some minutes mark the growth of cracks.

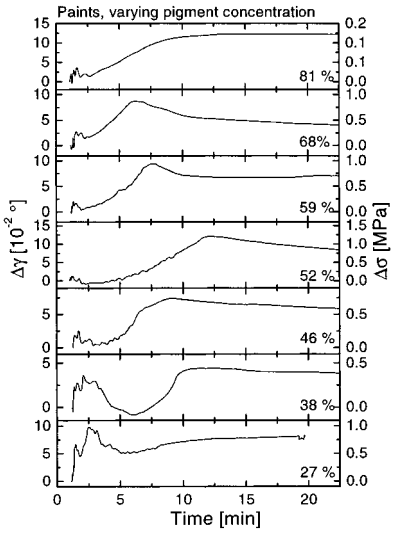

Figure 8. Stress history for drying of a pigment-loaded paint for varying pigment volume concentration. For high pigment concentration the binder forms patches between pigment particles but does not fill space, whereas for low pigment concentration the particles are dispersed in a matrix of the binder. The stress evolution suggests two separate processes, which are the drying of the polymer and the particle rearrangement to eliminate voids.

layer of particles, whereas the stress is still *dilational in the lower regions*. For very thin films, these lower regions hardly exist at all, and there is no dilational stress. The dilational stress observed for very thin films is indeed very weak (see bottom curve in Figure 6), which supports Sheetz' view.

The tensile stress observed in phase B is caused by the uniaxial shrinkage imposed by the substrate. It is always observed and even present in the case of conventional polymers. This effect, as well as the subsequent stress relaxation, (phase C) is well-known from everyday experience. The qualitative difference between phases A and B is that the volume of the particles now shrinks in phase B, while only changes of shape take place in phase A. It is again instructive to estimate the maximum tensile stress that can be exerted due to shrinkage, although the input parameters in this case are less certain than in the case of capillary pressure. We estimate the mismatch between the substrate dimension and the lateral dimensions of a hypothetical unconstrained film to be on the order of 5%. This corresponds to the amount of water which poly(vinyl acetate) takes up in humid atmosphere. The stress required to stretch the unconstrained film to the substrate dimensions is of the order of $0.05 \times E_f$ with E_f as the film's Young's modulus. An upper limit for the Young's modulus is obtained from Brown's well-known condition $G_f < 35\ \gamma_{WA}/R$, where G_f is the shear modulus of the latex particle, γ_{WA} is the air−water surface tension driving particle deformation, and R is the particle radius. Brown arrived at this condition by equating the stress exerted by the air−water interface to the stress exerted by the particles resisting deformation. Although the details of this calculation may be debated for various reasons, the general line of argument is undisputed. Because the interface tensions in question are all of the same order of magnitude, Brown's relation (with some margin on the number 35) should be quite general. With Brown's relation for the shear modulus using $R \approx 100$ nm and $E_f \approx 3\,G_f$ one arrives at σ_{max} in the order of 1 MPa. As the experimental results show, this is again in the right order of magnitude.

Figure 6 shows the dependence of the stress history on the film thickness. As expected, drying proceeds slower for larger film thickness. The overall magnitude of the equivalent stress decreases with increasing film thickness. Because the equivalent stress is an averaged quantity, this is indicative of internal stress heterogeneities. Presumably, most of the tensile stress is carried by a skin at the film−air interface. For the thin-film case, the skin extends over the entire film and the average stress equals the stress in the skin. For thicker films the softer bottom layer decreases the average stress.

Lateral tensile stress may even lead to cracks. This mode of failure of film formation is distinctly different from the inability of particles to deform. The "crack point", the temperature at which lateral stresses cause film formation failure, and the "white point", the temperature at which particle coalescence fails, are sometimes distinguishable on a temperature-gradient bar or "film formation bench."[34] Evidently, cracking is also reflected in the stress evolution. Figure 7 shows data obtained by the drying of the core−shell latex KR59 at various temperatures. This material cracks extensively when dried at a temperature less than 44 °C. Some of the cracks may also be located at the film−substrate interface and therefore be related to interfacial slippage. The temperature was adjusted with the base plate. The stress evolution is much less regular for this substance than for PVAc. We could not increase the base-plate temperature to the point at which the drying proceeded without these irregularities. A buildup of tension and subsequent relaxation is still observed. The buildup of tension, however, is interrupted by many cracks which show up as irregular depressions. The time scale of the crack-induced declinations is on the order of minutes. The evolution of the substrate bending presumably is determined by crack *growth* as opposed to crack nucleation. With further reduction in temperature, crack formation disappears again. A prerequisite for the buildup of cracks is the existence of a continuous film. Much below the MFT no such film forms, because particle deformation does not take place. There is no evidence of dilational stress in this set of experiments. At high temperatures the dilational stress may have been masked by the cracking events. At lower temperatures, dilational stress, if present, should have been observed. Possibly, the rigidity of the particles

(34) Winnik, M. A.; Wang, Y.; Haley, F. *J. Coat. Technol.* **1992**, *64*, 51.

prevents lateral stress. This would correspond the condition of a rigid skeleton of spheres (Poisson's number $\nu \approx 0$) which takes up vertical stress without diverting it to the side.

Finally, we present data on pigment-filled dispersions. With regard to the pigment concentration φ_{pg}, one usually distinguishes two different regions which are a $\varphi_{pg} \ll \varphi_c$ and $\varphi_{pg} \gg \varphi_c$, where $\varphi_c \sim 55\%$ is the critical pigment volume concentration (CPVC). For $\varphi_{pg} \ll \varphi_c$ the particles are well dispersed in the matrix, and for $\varphi_{pg} \gg \varphi_c$ the polymer cannot fill the voids between the pigment particles but rather forms patches between neighboring spheres, the rest of interstitial volume being filled with air. The regime $\varphi_{pg} \sim \varphi_c$ is considered unfavorable in application because of the buildup of large stresses. Although one might expect numerous cracking events at $\varphi_{pg} \sim \varphi_c$, Figure 8 shows that this is not actually the case. Rather, the stress history becomes bimodal with two well-separated maxima of tensile lateral stress at a filler content φ_{pg} somewhat less than φ_c. Although the detailed interpretation would require more structural information, the stress evolution lends itself to a picture with two distinct phases, one connected to a structural reorganization of filler particles to reduce the interstitial volume and the other phase dominated by drying of the polymeric binder.

Conclusions

The evolution of macroscopic lateral stress during drying of latex spheres reflects internal micromechanical processes of considerable complexity. We find evidence of lateral dilational stress, which we attribute to the capillary pressure according to the Sheetz model. After the end of stage II, the stress becomes tensile because of the uniaxial shrinkage imposed by the substrate. Cracking leads to stress minima on the time scale of minutes, and the stress evolution here is governed by crack growth rather than crack nucleation. The stress evolution of pigment-filled layers is bimodal, indicative of separate time scales for relaxation of the polymeric matrix and the ensemble of filler particles.

Acknowledgment. We thank Alexander Du Chesne and Thorsten Thürrigl for numerous discussions and technical help. C.P. acknowledges a fellowship from the Center for Polymeric Interfaces and Macromolecular Assemblies (CPIMA) under contract DMR 9400354. Part of this work was funded by BMBF project FKZ 03N3018 A 5.

LA990256M